Journal of Power Sources 208 (2012) 86–95

Contents lists available at SciVerse ScienceDirect

Journal of Power Sources

journal homepage: www.elsevier.com/locate/jpowsour

Screen-printed $(La,Sr)CrO_3$ coatings on ferritic stainless steel interconnects for solid oxide fuel cells using nanopowders prepared by means of ultrasonic spray pyrolysis

Tomasz Brylewski[a,*], Jaroslaw Dabek[a], Kazimierz Przybylski[a], Jerzy Morgiel[b], Mieczyslaw Rekas[a]

[a] AGH University of Science and Technology, Faculty of Materials Science and Ceramics, Al. Mickiewicza 30, 30-059 Cracow, Poland
[b] Institute of Metallurgy and Materials Science, Polish Academy of Science, 25 Reymonta St., 30-059 Cracow, Poland

ARTICLE INFO

Article history:
Received 3 December 2011
Received in revised form 24 January 2012
Accepted 5 February 2012
Available online 13 February 2012

Keywords:
SOFC
Metallic interconnect
Ferritic stainless steel
Coating
Chromia scale
$(La,Sr)CrO_3$ perovskite

ABSTRACT

In order to protect the cathode from chromium poisoning and improve electrical resistance, a perovskite $(La,Sr)CrO_3$ coating was deposited on the surface of a DIN 50049 ferritic stainless steel by means of the screen-printing method, using a paste composed of an ultra-fine powder prepared via ultrasonic spray pyrolysis. Investigations of the oxidation process of the coated steel in air and the $Ar–H_2–H_2O$ gas mixture at 1073 K for times up to 820 h showed high compactness of the protective film, good adhesion to the metal substrate, as well as area specific resistance (ASR) at a level acceptable for metallic SOFC interconnect materials. The microstructure, nanostructure, phase composition of the thick film, and in particular the film/substrate interface, were examined via chemical analyses by means of SEM-EDS and TEM-SAD. It was shown that the $(La,Sr)CrO_3$ coating interacts with the steel during long-term thermal oxidation in the afore-mentioned conditions and intermediate, chromia-rich and/or spinel multilayer interfacial zones are formed. Cr-vaporization tests showed that the $(La,Sr)CrO_3$ coating may play the role of barriers that decrease the volatilization rate of chromia species.

1. Introduction

Solid oxide fuel cells (SOFCs) are highly promising tools that might become efficient sources of electrical energy and heat in the future. The construction of the planar-type SOFC needs bipolar interconnects for separating fuel and air flow, and to provide electrical contact and mechanical stabilization of the cell in a stack [1]. Reducing SOFC operating temperatures to the 923–1073 K range makes it possible to employ cost-effective metallic interconnects such as ferritic stainless steel (FSS) instead of the standard ceramic materials applied thus far, mainly doped lanthanum chromite [2–7]. The key issues in the application of chromia-forming steels in SOFCs are: their corrosion resistance in oxidizing/reducing atmospheres, which is related to the growth of a protective chromia scale, the compatibility of their thermal behavior with that of solid electrolytes of doped-ZrO_2 (zirconia-based electrolytes) and doped-CeO_2 (ceria-based electrolytes), and the need to obtain better mechanical properties [1].

Review papers [7–11] clearly show that the currently used ferritic stainless steel interconnects with >20 wt.% chromium content are unsuitable for practical applications in solid oxide fuel cells operating at intermediate temperatures (IT-SOFC). Their area specific resistance (ASR), defined as the product of resistance and nominal contact surface area of the oxide and steel, increases in time due to the growing thickness of the semiconducting chromia layer, and does not meet the requirements set for SOFC applications (ASR lower than 0.1 $\Omega\,cm^2$). The second problem encountered with chromia is their potential transformation into volatile chromium species such as $CrO_2(OH)_2$ or CrO_3, leading to the loss of their protective properties and the poisoning of cathode material, and the subsequent degradation of the fuel cell [12–15]. Tests carried out on a ferritic stainless steel in a dual atmosphere (one side exposed to air and the other side exposed to $H_2–H_2O$) showed that scale growth was significantly different from that in a single atmosphere [16]. Oxygen reacts with the interconnect to form oxides, whereas hydrogen can migrate across the interconnect and into the metal, causing embrittlement and leading to the detrimental presence of hydrogen at the metal-oxide interface and in the oxide scale formed on the air side [17].

Consequently, the application of ferritic stainless steels requires their surface to be modified in order to guarantee durability and reliability. Relatively dense inorganic materials including La-based perovskites [7,8,10,18,19], Mn-based spinels [9,10,20], oxidation-resistant systems of MAlCrYO (M represents a metal, e.g. Co, Mn and/or Ti) [21] and reactive element oxides (REOs) [6,22,23] may be applied on ferritic stainless steels as protective and conducting

* Corresponding author. Tel.: +48 126172469; fax: +48 126172493.
E-mail address: brylew@agh.edu.pl (T. Brylewski).

0378-7753/$ – see front matter © 2012 Elsevier B.V. All rights reserved.
doi:10.1016/j.jpowsour.2012.02.015

coatings. Such modification makes it possible for the layered substrate made of heat-resistant steel with a protective-conductive coating to achieve low electrical surface resistance that does not change in time, high resistance to cyclic thermal oxidation, and to effectively prevent chromium migration from the chromium-containing steel substrate.

Due to its relatively high chemical stability under an oxygen partial pressure gradient, thermal expansion match and high electronic conductivity at operating temperatures from 973 to 1273 K, the Sr-doped lanthanum chromite (La,Sr)CrO_3 has been among the materials used for coating [13,24,25]. A variety of methods for depositing ceramic coatings based on this material on ferritic steels and their physicochemical properties have been reported [18,19,26–33]. One of the simpler methods that may be used to fabricate thick, polycrystalline (La,Sr)CrO_3 films is the cost-effective screen-printing technique followed by appropriate thermal treatment [7,33,34]. Nevertheless, to obtain a highly dense coating that adheres well to the substrate, it is recommended to use nanostructured powders in the form of spherical particles, the surfaces of which will constitute the approximation of the 2D structure. In this respect the ultrasonic spray pyrolysis (USP) method for the preparation of ultra-fine (La,Sr)CrO_3 powders is of particular interest.

To understand how the surface stability of the applied steels is affected and how the electrical performance of ceramic/composite materials in SOFCs operating at about 1073 K may be improved, it is necessary to obtain information on the microstructure of the product of the reaction between the conductive oxide coating and the metallic substrate that takes place at their interface: this is the key issue with regard to the application of steel as an interconnect in SOFCs.

In this paper we present the detailed preparation of a highly compact (La,Sr)CrO_3 thick film on a DIN 50049 ferritic stainless steel, obtained by means of the screen-printing method using a paste composed of ultra-fine powder prepared via ultrasonic spray pyrolysis. The oxidation kinetics of uncoated and coated steel in air and the Ar–H_2–H_2O mixture were studied. The post-oxidation phase, chemical composition, morphology and nanostructure of the coatings were investigated, with particular focus on the coating/metal substrate interface, and the influence of the interface reactions between the conductive ceramic layers and the steel substrates was discussed in terms of electrical properties and chromium vaporization rate.

2. Experimental

2.1. Preparation of steel samples

The material used for the experiments was the commercial DIN 50049 ferritic steel from Valcovny Plechu a.s. Frydek-Mistek, Czech Republic, with the chemical composition of: Fe (Bal.), Cr (24.55 mass%), Mn (0.28 mass%), Si (0.74 mass%), Ni (0.99 mass%), C (0.04 mass%). Steel coupons in the form of rectangular plates with the dimensions 10 mm × 20 mm × 0.5 mm were cut from the supplied material. For oxidation tests, the surfaces of all specimens were ground with 100–1000-grid SiC papers, then polished with a 0.3 μm alumina slurry (OP-U Struers, Denmark), ultrasonically degreased and finally washed in acetone and ethanol immediately prior to each use.

2.2. Preparation of (La,Sr)CrO_3 nanopowder and methods of its characterization

A powder of the nominal composition $La_{0.8}Sr_{0.2}CrO_3$ was prepared using the ultrasonic spray pyrolysis (USP) method described elsewhere [35]. Fig. 1 shows the scheme of the apparatus. Aqueous solutions of lanthanum, strontium and chromium nitrates with 0.2 M (M-molar concentration mol dm^{-3}) concentration were mixed together in an appropriate ratio to yield the desired stoichiometry. The obtained mixture with 0.08 M concentration was introduced (at a rate of 5 cm^3 min^{-1}) into an ultrasonic nebulizer working at a frequency of 2.6 MHz using a peristaltic pump. The obtained aerosol was then transported into the reaction tube placed in a two-heat zone furnace, using the Ar–15%H_2 mixture as the carrier gas. Aerosol particles were thermally decomposed in the first reaction zone, under 1023 K. The obtained particles were separated from the carrier gas by means of a titanium electrostatic filter placed in the second heat zone with a temperature of 573 K. The resulting powder was then calcined in air at 1023 K for 1 h.

The phase composition of the obtained chromite powder was analyzed by means of X-ray diffraction using a Philips X'Pert XRD. Powder morphology was investigated using the FEI Nova NanoSEM 30 scanning electron microscope coupled with EDAX Genesis XM X-ray microanalysis system and by means of conventional transmission electron microscopy (TEM) and selected-area diffraction (SAD) using Philips CM 20 at 200 kV. The chemical composition of the obtained powder was determined using atomic absorption spectroscopy (ASA) using the Pye Unicum SP90B spectrometer.

2.3. Paste preparation and coating process

DIN 50049 ferritic steel substrates were coated with the (La,Sr)CrO_3 paste by means of the screen-printing method. The pastes were prepared by mixing the $La_{0.8}Sr_{0.2}CrO_3$ powder and a 5 wt.% solution of ethyl cellulose in terpineol. The mixture, containing about 17 wt.% of organic binder, was homogenized for 10 h in a three-roller mixer. The viscosity of the paste was in the range between 4 and 5 Pa s at a room temperature. Thick films were deposited on abraded (600-grid SiC) surfaces of steel substrates using a 100 mesh screen. To obtain coatings of different thickness, printing was repeated one to two times. The films were then dried at 353 K for 2 h. The organic components were removed entirely from the paste by thermally annealing the coated specimens in air at 1073 K for 30 min. The thickness of the deposited films was about 20–40 μm.

2.4. Oxidizing procedure and methods of sample characterization

The oxidation kinetics of coated and uncoated DIN 50049 steels were investigated under isothermal conditions at 1073 K for up to 300 h in dry, flowing air and in a controlled Ar–H_2–H_2O gas mixture, with $p_{H_2}/p_{H_2O} = 94/6$, using a thermogravimetric apparatus with a MK2-G5 Vacuum Head Microbalance (CI Electronics Ltd., UK) with a sensitivity of 10^{-6} g. The high-temperature thermogravimetric apparatus and the preparation procedure of the Ar–H_2–H_2O gas mixture have been described previously [36].

The area specific resistance (ASR) vs. time measurements for coated and uncoated steel were conducted using a four-probe DC technique under a constant current density of 0.1 A cm^{-2} in air and the Ar–H_2–H_2O gas mixture at 1073 K, using the setup shown in Fig. 2. The apparatus and the methods used for measuring ASR and sample preparation are described in [37].

Chromium vaporization rate tests of the studied samples were performed in humidified air ($p_{H_2O} = 9.72 \times 10^{-2}$ atm) at 1073 K for 72 h in an apparatus of a construction similar to the one proposed by Kurokawa et al. [14]. The details of the apparatus used for Cr-vaporization rate tests and the preparation procedure of the air–H_2O gas mixture have been described previously [15]. The concentration of chromium in the obtained aqueous solution containing the dissolved Cr was determined by means of the atomic absorption spectroscopy method.

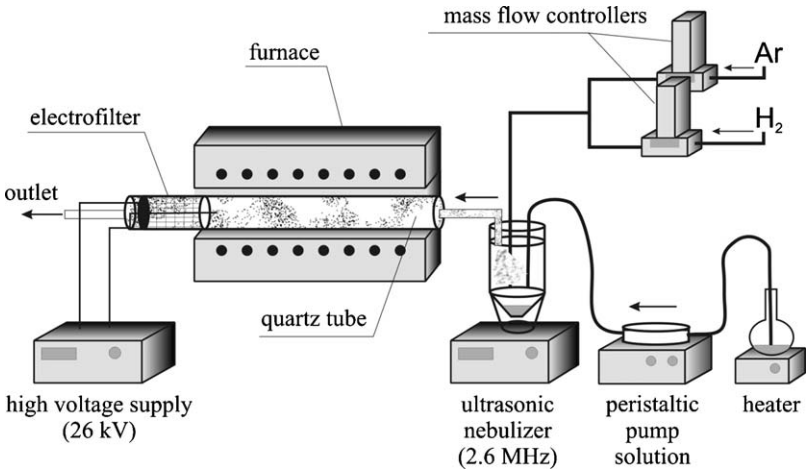

Fig. 1. Scheme of the ultrasonic spray pyrolysis (USP) apparatus [35].

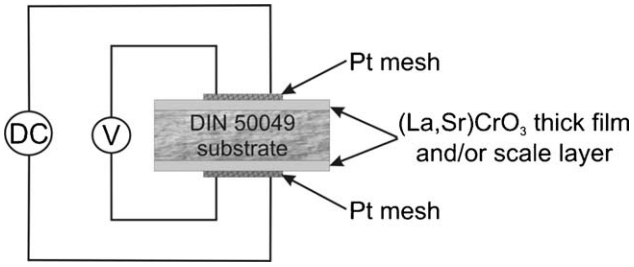

Fig. 2. Schematic diagram of ASR measurement setup utilizing the four-probe DC method.

The phase composition of the oxidized samples was analyzed by means of X-ray diffraction. SEM-EDS and conventional TEM-SAD in both plan- and cross-sectional views were used to examine the morphology and nanostructure of the oxide scales grown on uncoated and coated substrates in detail. Electron-transparent thin foils were prepared by dimpling with a Gatan Dimpler and ion-milled with a Gatan DuoMill 600 with 5 kV argon ions at the incidence angle of 15°.

3. Results and discussion

3.1. (La,Sr)CrO_3 powder characteristics

As a result of the optimization of spraying and thermal treatment of aerosols nanospherical particles of (La,Sr)CrO_3 powder with the desired phase and chemical composition were obtained. Fig. 3 shows an X-ray diffraction pattern of the (La,Sr)CrO_3 powder obtained using the USP method followed by thermal treatment in air at 1023 K.

Based on the ex situ X-ray analysis of the (La,Sr)CrO_3 phase composition it may be concluded that the studied material has a single-phase structure. The numerical Rietveld analysis of the obtained spectra indicates the presence of a perovskite phase in the powders; this phase appears to crystallize in the ideal cubic structure with the Pm-3m space group. The established values of lattice parameters, $a = b = c = 0.38428(5)$ nm, are consistent with reference data [38]. Deviations from nominal stoichiometry (La:Sr:Cr = 0.8:0.2:1.0) of the prepared powder were analyzed by means of ASA. It was found that the examined powder had a molar ratio La:Sr:Cr = 0.80:0.21:1.06. These results prove that using USP it is possible to obtain a fully reacted (La,Sr)CrO_3 perovskite at the relatively low temperature of 1023 K; the same cannot be said of many low-temperature methods used to synthesize chromite ceramic materials characterized by low sinterability.

Fig. 4(a) and (b) presents TEM images of the particles of the studied nanopowder obtained by means of USP followed by thermal treatment in air atmosphere at 1023 K for 1 h. As can be seen, the examined (La,Sr)CrO_3 powder contains mainly spheres 350–1600 nm in diameter. These particles are built of equal-sized grains about 10–15 nm large, which is consistent with the 14 nm crystallite size estimated based on the analysis of X-ray line broadening according to Scherrer's formula [39]. Regardless of size, all spheres have a thickness of around 30 nm. The sphere walls show slight irregularities, but they generally maintain their spherical shape (Fig. 5(a)). Electron diffraction carried out for the analyzed spheres, performed in a parallel beam by means of the SADP technique (Fig. 5(b)), indicates that they are built of (La,Sr)CrO_3 nanocrystals of perovskite structure crystallizing in a regular system (visible fourfold axes).

Local EDS chemical analysis with a nominal probe size of 5 nm (Fig. 5(c)) and mapping indicated that the distribution of the La,Sr and Cr elements on the surface of the nanospherical particles was homogeneous and that the stoichiometric ratio of these elements was 0.8:0.2:1.0, which agrees well with the findings from the chemical analysis using ASA.

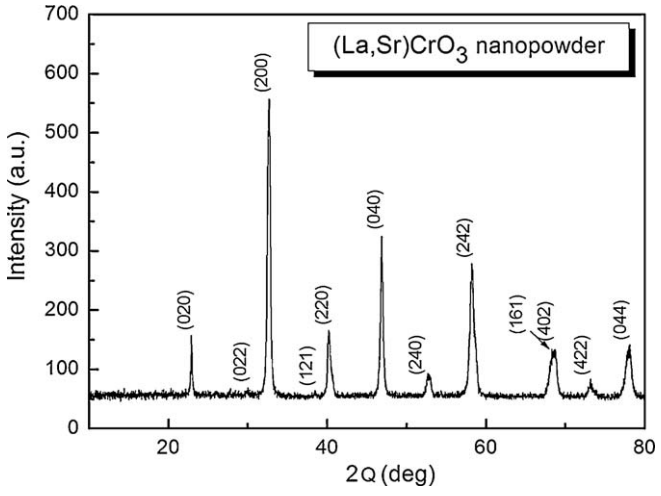

Fig. 3. X-ray diffraction pattern of the (La,Sr)CrO_3 powder obtained via USP.

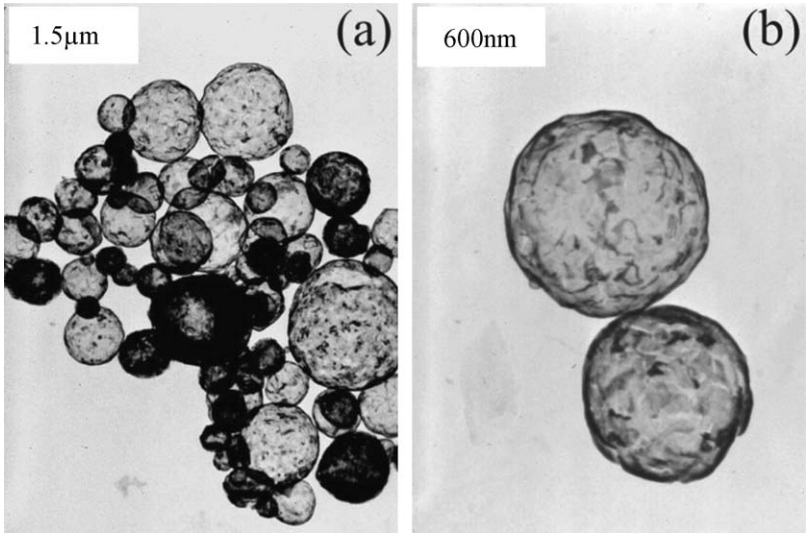

Fig. 4. (a) and (b) TEM images of $(La,Sr)CrO_3$ particles synthesized via USP.

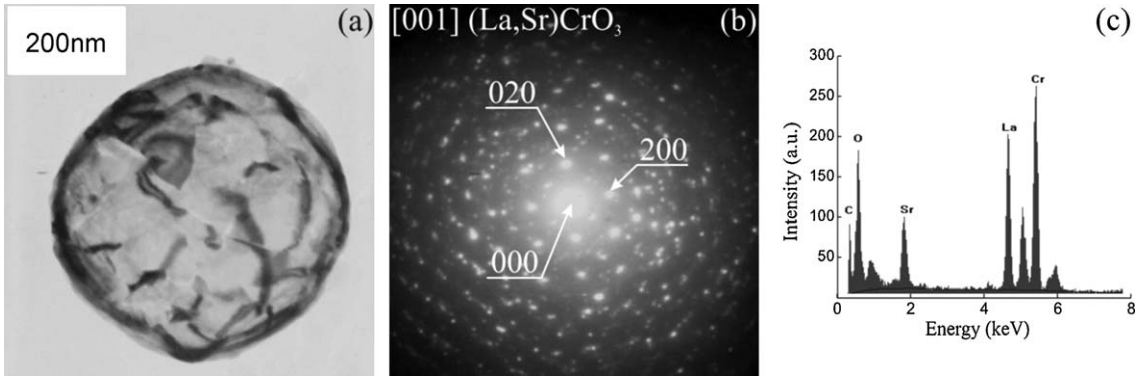

Fig. 5. TEM images of: (a) $(La,Sr)CrO_3$ particles, (b) SADP diffraction pattern with [0 0 1] $(La,Sr)CrO_3$ zone axis and (c) EDS analysis of the surface.

3.2. Oxidation kinetics of the product and its microstructure

One of the important requirements for metallic interconnects to be exposed to oxidizing/reducing SOFC atmospheres at 1073 K is good resistance against high-temperature corrosion. In order to compare oxide scale growth rates between the coated and uncoated samples, the weight gain per unit area ($g\,cm^{-2}$) vs. annealing time was measured using isothermal thermogravimetric analysis. For comparison, the thickness of the oxide scale formed on the uncoated steel surface and the one formed between the coating and the metallic substrate was also determined by examining microsections using microscopy.

Fig. 6 illustrates the kinetics of isothermal oxidation of the DIN 50049 steel, uncoated and coated with the $(La,Sr)CrO_3$ thick film at 1073 K in air and the Ar–H_2–H_2O gas mixture with p_{H_2}/p_{H_2O} = 94/6. The presented kinetic curves do not take the mass loss related to the formation of volatile chromium compounds into account. The corresponding relative error for times shorter than 1200 h does not exceed 3%. The effective thickness values of the reaction products, calculated from the determined parabolic rate constants for uncoated and coated ferritic steel, are within 6% of the values observed in metallographic observations. When calculating scale thickness from the weight change, a pure chromia scale was therefore assumed. As can be seen, the oxidation process of the studied samples approximately obeyed the parabolic rate law. The observed irregularities in the kinetic profiles are due to mass losses resulting from scale or/and film spallation during oxidation. The calculated parabolic rate constants for the oxidation of both studied samples at 1073 K were of the order of 10^{-13}–10^{-15} $g^2\,cm^{-4}\,s^{-1}$, typical of "*chromia formers*" [40]. The experimental kinetic data obtained in this study, including sample treatment atmosphere, parabolic rate constant (k_p), correlation coefficients (r) from the regression analysis, and the time intervals (t) in which the parabolic rate law is obeyed are collected in Table 1. The comparison of these data shows that the DIN 50049 steel coated with $(La,Sr)CrO_3$ thick film exhibited good oxidation properties in comparison with the

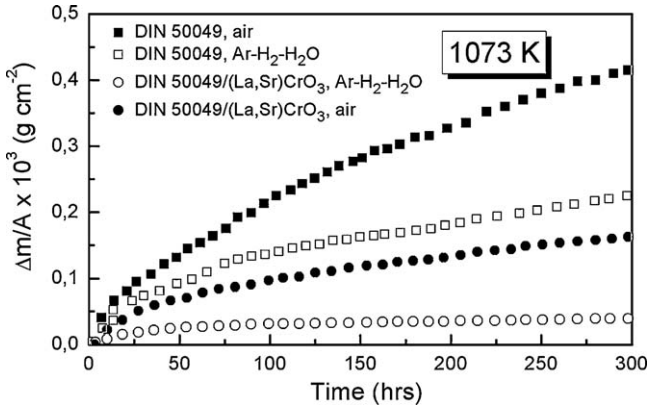

Fig. 6. Oxidation kinetics of DIN 50049 steel, uncoated and coated with $(La,Sr)CrO_3$ thick film at 1073 K in air and Ar–H_2–H_2O.

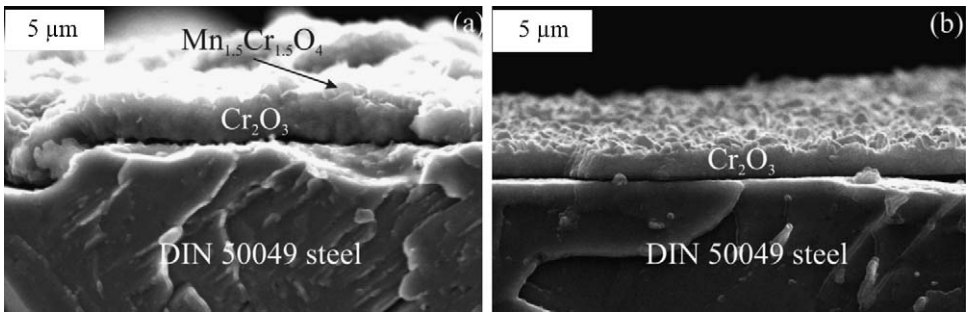

Fig. 7. SEM-SE micrographs of fracture cross-sections through the scale formed on uncoated DIN 50049 steel at 1073 K for 550 h in: (a) air and (b) Ar–H_2–H_2O.

uncoated steel in both reaction atmospheres. It may thus be said that the screen-printed coating greatly inhibits oxide scale growth by reducing the supply of oxygen needed for the growth of chromia through the (La,Sr)CrO_3 thick film (transport via oxygen vacancies). It should be noted that the parabolic rate constant of the oxide product growth in the Ar–H_2–H_2O gas mixture is about one order of magnitude lower than that of the sample oxidized in air (Table 1). This observation is confirmed by others [7,40].

Long-term growth of a chromia scale on the uncoated DIN 50049 steel in air and the Ar–H_2–H_2O gas mixture at 1073 K for up to 550 h leads to the deterioration of scale compactness due to the outward diffusion of chromium ions, which may cause porosity at the steel/scale interface and, when combined with significant growth stress, may result in scale spallation. Fig. 7(a) and (b) shows the typical morphology of an oxide scale formed on the uncoated DIN 50049 steel after oxidation in air and the Ar–H_2–H_2O gas mixture at 1073 K for 550 h. The scales developed on the steel in air were composed mainly of Cr_2O_3 doped with Fe as an inner layer, while the continuous outer thin layer was composed of $Mn_{1.5}Cr_{1.5}O_4$ spinel, which partially suppressed chromium vaporization; this phenomenon will be addressed later on. Similar phases were also observed on the surface of other Mn-containing Fe–Cr alloys [2,5,41]. In the case of the uncoated steel oxidized in the Ar–H_2–H_2O gas mixture, the main oxidation product was a chromia layer in the form of ridges, shaped by water vapor and hydrogen acting on the defect structure in chromia scale [2,41]. On the top of the Cr_2O_3 layer, a $Mn_{1.5}Cr_{1.5}O_4$ spinel in the form of non-continuous layers and nodules of crystallite was observed. Moreover, isolated amorphous silica formed as a result of selective oxidation of Si were found at the scale/substrate interface (Fig. 8(a) and (b)). The ferritic steels that contain Si in amounts greater than 0.5 wt.% usually form insulating, network-like films of silica, which may grow under the chromia scale [42]. The existence of these phases in the double-layered chromia scales, confirmed by XRD and EDS analyses, was predicted based on thermodynamic calculations [43]. Fig. 9 illustrates oxygen partial pressure equilibrium as a function of temperature for NiO, FeO, Cr_2O_3, MnO, SiO_2, $FeCr_2O_4$ and $MnCr_2O_4$ phases, taking into account steel composition (Table 1) calculated from the available thermodynamic data [43,44] and assuming an ideal model of the steel. The oxygen partial pressure of Ar–H_2–H_2O gas mixture with a value of $p_{H_2}/p_{H_2O} = 94/6$ is also included.

Table 1
Parabolic rate constants of DIN 50049 steel, uncoated and coated with the (La,Sr)CrO_3 film oxidized at 1073 K in different atmospheres.

Sample	Atmosphere	t (h)	k_p ($g^2\,cm^{-4}\,s^{-1}$)	r
DIN 50049	Air	50–300	1.7×10^{-13}	0.9993
DIN 50049	Ar–H_2–H_2O	50–300	3.3×10^{-14}	0.9977
DIN 50049/(La,Sr)CrO_3	Air	50–300	2.0×10^{-14}	0.9988
DIN 50049/(La,Sr)CrO_3	Ar–H_2–H_2O	10–300	8.4×10^{-16}	0.9964

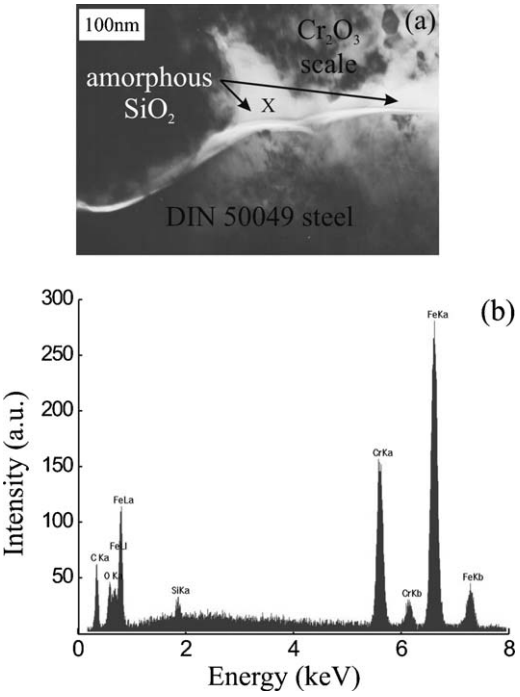

Fig. 8. (a) TEM cross-section micrograph showing isolated amorphous silica formed at the scale/substrate interface and (b) EDS point microanalysis for regions designated as X.

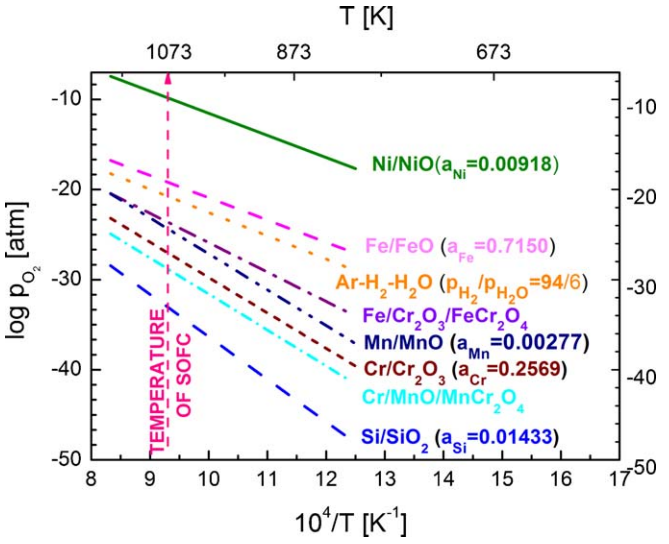

Fig. 9. Oxygen pressure equilibrium as a function of temperature for several phases taking into account steel composition.

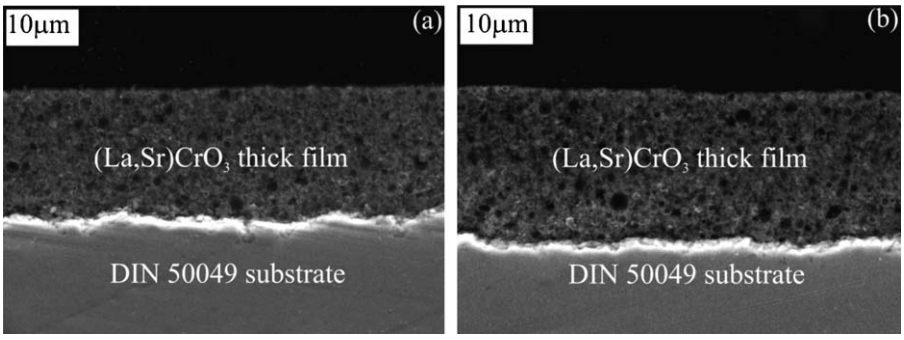

Fig. 10. SEM-SE cross-section micrographs of the oxidized DIN 50049 steel coated with $(La,Sr)CrO_3$ at 1073 K for: (a) 820 h in air and (b) 760 h in $Ar–H_2–H_2O$ [33].

The reason for the accelerated corrosion of uncoated DIN 50049 steel in air at 1073 K (Fig. 6) is the formation of a thick and continuous spinel outer-layer, related to the very fast diffusion of manganese in the chromia scale [45]. Spallation and cracking of the scale due to the mismatching of its thermal expansion coefficient with that of the metal core, which lead to the formation of diffusion paths for cations and anions, may also increase the growth rate of the oxide scale [41]. The exposition of the DIN 50049 steel to the $Ar–H_2–H_2O$ mixture generally yields better adhesion of oxidation products than exposition to air (Fig. 7a). This has been confirmed by other authors [2,41,46]. In addition, a certain amount of silica precipitates at the scale/steel interface boundary, which blocks the flux of chromium into the reaction zone interface, and therefore decreases the oxidation rate of uncoated steel in the $Ar–H_2–H_2O$ gas mixture. However, such chromia scales grown thermally on uncoated ferritic steel in both atmospheres exhibit poor electrical conductivity, which may increase overall cell resistance during long-term operation, as will be shown in the next subsection.

In order to improve the corrosion resistance of the studied steel and simultaneously increase electrical conductivity of the chromia scale for long exposure times in SOFC operating conditions, a thick film of conducting $(La,Sr)CrO_3$ was deposited on the surface of the DIN 50049 steel using the screen-printing method. Fig. 10(a) and (b) shows SEM micrographs of the polished cross-section of the DIN 50049 steel coated with $(La,Sr)CrO_3$ film after oxidation at 1073 K in both air and $Ar–H_2–H_2O$ gas mixture atmospheres [33]. These figures confirm the very good adhesion of the thick films to the metal core and demonstrate their small porosity. This is because their thermal expansion coefficient matched that of the substrate well. The TEC of $La_{0.8}Sr_{0.2}CrO_3$ ($10.90 \times 10^{-6}\,K^{-1}$) is relatively close to the TEC values of DIN 50049 ferritic steel ($11.33 \times 10^{-6}\,K^{-1}$) [4,24]. The thickness of the coatings ranged from about 20 μm to 30 μm. The cavities visible in the oxide coating originate from $(La,Sr)CrO_3$ powder nanospheres presented in Fig. 4(a) and (b). SEM micrographs did not reveal any essential differences in grain size of $(La,Sr)CrO_3$ coatings for the two examined $(La,Sr)CrO_3$/DIN 50049 composites (Fig. 10(a) and (b)).

Detailed cross-sectional SEM-EDS and TEM-SAD investigations of the DIN 50049 steel coated with conducting $(La,Sr)CrO_3$ film oxidized in the afore-mentioned conditions revealed the presence of an interfacial zone of about 1–2 μm. These layers developed between the film and the metallic core have a complex multilayer structure with a composition dependent on the thermal treatment atmosphere. It may be assumed that the existence of the intermediate layer, which relaxes the thermal strain at the coating/steel interface, improves scale adhesion. Table 2 lists the phase compositions in the DIN 50049 steel coated with $(La,Sr)CrO_3$ thick film oxidized at 1073 K in different atmospheres, taken from the conducting layers successively thinned by abrading down to the metal substrate. As a result of oxidation of the $(La,Sr)CrO_3$/DIN 50049 in air at 1073 K, $SrCrO_4$ precipitates were detected in the $La_{0.8}Sr_{0.2}CrO_3$ coating (Table 2). This is connected with the low solubility of Sr in the $LaCrO_3$ perovskite [47]. The thermochemical calculations presented in [48] indicate that $La_{0.8}Sr_{0.2}CrO_3/SrCrO_4$ reaches phase equilibrium in air at 1073 K. The bottom portion of the intermediate layer close to the metal substrate of the studied composite exposed to air is built of a continuous Cr_2O_3 layer and a non-continuous $(Mn,Fe)Cr_2O_4$ spinel layer, while the upper part of the spinel appeared in the additional thin, non-continuous layer of $LaCrO_3$ (Table 2).

Moreover, as a result of the chemical interactions between the constituents of the $La_{0.8}Sr_{0.2}CrO_3$ coating and the Cr_2O_3 layer on the metallic core, precipitates of the $SrCrO_4$ compound are formed next to the $LaCrO_3$ phase at the coating/steel interface, according to the following reaction:

$$5La_{0.8}Sr_{0.2}CrO + \frac{1}{2}O_2 \Leftrightarrow SrCrO_4 + 4LaCrO_3 \quad (1)$$

The above reaction process corresponds well to the analysis of the $SrO–Cr_2O_3–La_2O_3$ phase diagram presented by Peck et al. [47].

The nature and distribution of these phases in the $(La,Sr)CrO_3$/DIN 50049 composite exposed to air at 1073 K were investigated using TEM-SAD analysis. Fig. 11(a) shows a TEM image of a fragment of the studied composite with visible coating/intermediate reaction layer and intermediate reaction

Table 2
Phase composition in the DIN 50049/$(La,Sr)CrO_3$ composite after oxidation at 1073 K in different atmospheres, as determined using XRD analyses.

Atmosphere	Oxidation time (h)	Analyzed part of the coating/steel material		
		Outer film surface	Inside layer near the reaction product	Reaction layer near the metal core
Air	820	$La_{0.8}Sr_{0.2}CrO_3$ $SrCrO_4$	$LaCrO_3$ $SrCrO_4$ $(Mn,Fe)Cr_2O_4$	Cr_2O_3 $(Mn,Fe)Cr_2O_4$ $SrCrO_4$
$Ar–H_2–H_2O$	760	$La_{0.8}Sr_{0.2}CrO_3$	$LaCrO_3$ $(Mn,Fe)Cr_2O_4$	$(Mn,Fe)Cr_2O_4$ $SrCrO_4$ $Sr_2LaFe_3O_{8.94}$ Trace Cr_2O_3

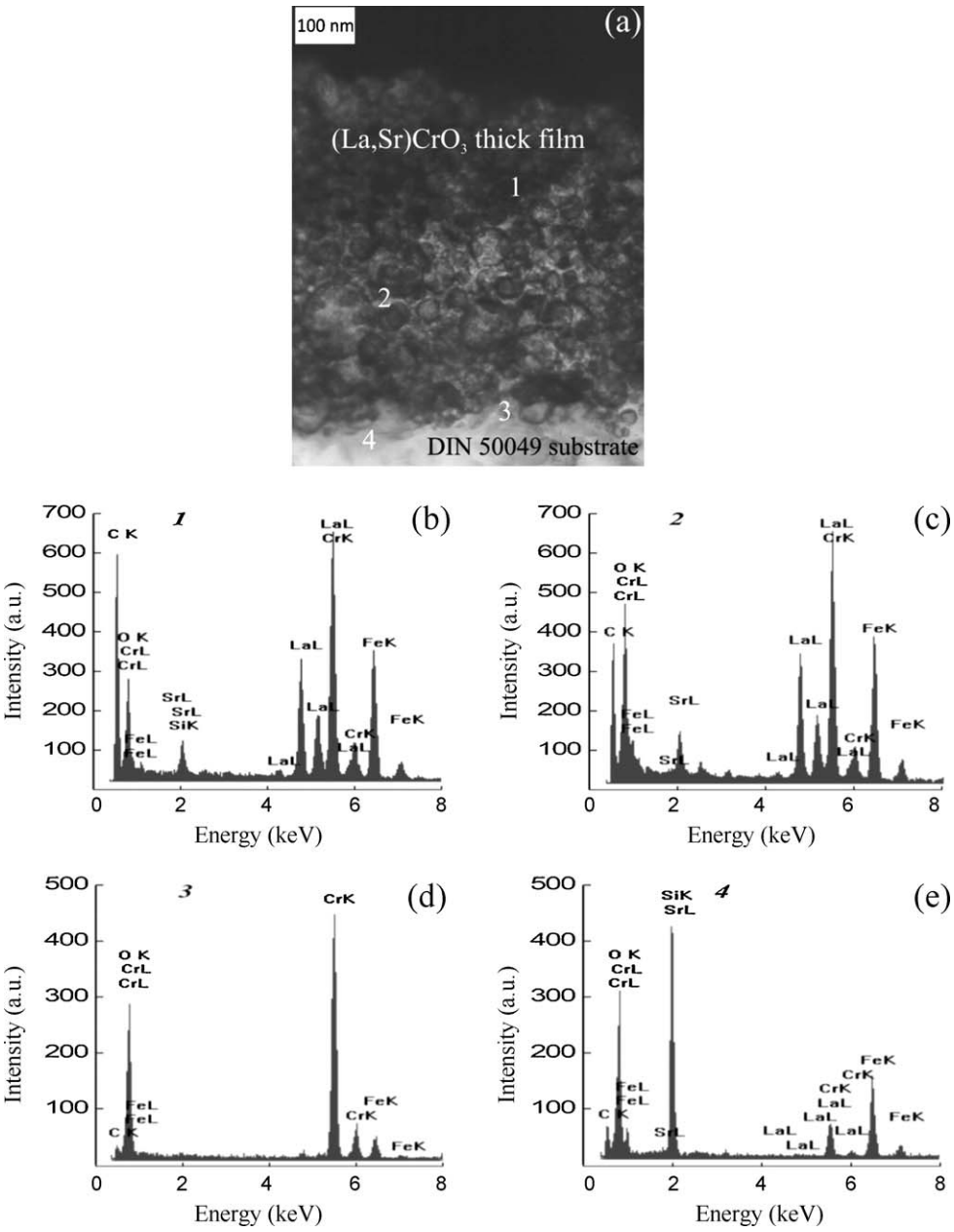

Fig. 11. (a) TEM cross-section micrograph of the multilayer oxide/metal interface between the (La,Sr)CrO_3 coating and the DIN 50049 substrate of the (La,Sr)CrO_3/DIN 50049 composite oxidized at 1073 K in air for 820 h, (b), (c), (d) and (e) EDS point microanalyses of regions designated as 1, 2, 3 and 4.

layer/metallic core interfaces, the position of which was determined based on EDS line scan analysis and a series of EDS point analyses presented in Fig. 11(b)–(e). When comparing the results of these analyses carried out in the upper part of the coating (region *1* – Fig. 11(b)) and its lower part, which is directly adjacent to the intermediate reaction layer (region *2* – Fig. 11(c)), similarity between their chemical composition and particle shape may be observed. The interaction product formed after the oxidation of (La,Sr)CrO_3/DIN 50049 composite in air was composed of a 1 μm thick continuous Cr_2O_3 layer formed from fine-crystalline grains ca 15 nm to 80 nm in diameter (region *3* – Fig. 11(d)). In addition, there was some non-continuous precipitation of the (Mn,Fe)Cr_2O_4 spinel in some areas of this layer, and it was separated by amorphous inclusions of SiO_2 that were embedded in the intergrain boundaries of chromium oxide (region *4* – Fig. 11(e)). Precipitates of the $SrCrO_4$ phase were also observed in these boundary regions.

Oxidation of the studied DIN 50049 steel coated with (La,Sr)CrO_3 in Ar–H_2–H_2O gas mixture at 1073 K for 760 h leads to the formation of a thin, continuous (Mn,Fe)Cr_2O_4 spinel layer at the coating/steel interface, which proceeds along with the diffusion of manganese from the steel to the interfacial zone; trace amounts of chromia are present in this area (Table 2). Subsequently, it may assumed that Cr_2O_3 acts as one of the substrates in the reaction in which the $SrCrO_4$ phase is formed according to equation (1). The latter phase is also thermodynamically stable in the Ar–H_2–H_2O gas mixture, in which the partial pressure of oxygen at 1073 K is equal to 1.6×10^{-21} atm. The EDS line scan analysis of La, Cr, Fe, Sr, Si and O across the cross section of the intermediate layer in the (La,Sr)CrO_3/DIN 50049 composite (Fig. 12(a)), shown in Fig. 12(b), confirms the afore-mentioned considerations. Moreover, $Sr_2LaFe_3O_{8.94}$ precipitates as a "*Ruddlesden-Popper phase*" near the metal substrate enriched with small particles of silica were found

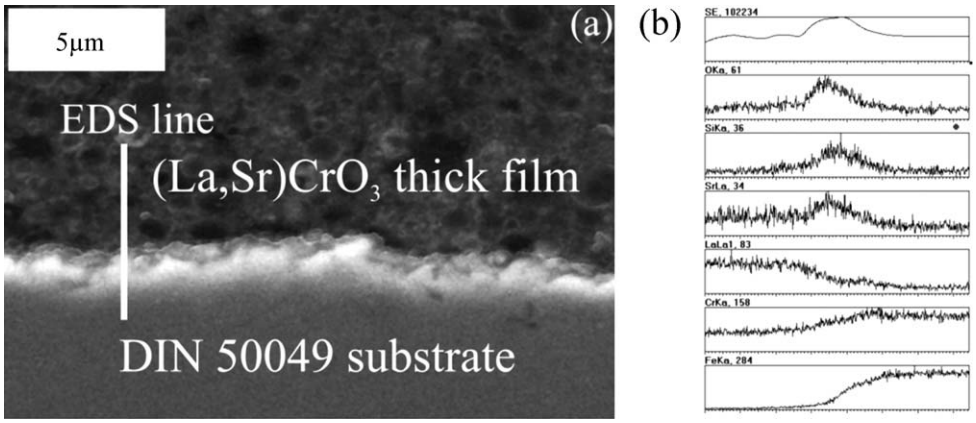

Fig. 12. (a) SEM-SE cross-section micrograph and (b) EDS line scan images across the multilayer (La,Sr)CrO_3/DIN 50049 interface formed after oxidation in Ar–H_2–H_2O at 1073 K for 760 h, along the white line in (a).

in the interaction layer (Table 2). This seems to explain why the observed oxidation parabolic rate constant is over one order of magnitude lower than its value predicted based on the oxidation kinetics of the (La,Sr)CrO_3/DIN 50049 composite in air (Table 1).

3.3. Application of the DIN 50049 ferritic steel in SOFC interconnects

The low area specific resistance of the thermally grown chromia scale and the suppression of chromium vaporization from the oxidized scale are other important requirements set for SOFC metallic interconnect.

In order to determine the electrical resistance and evaluate the usefulness of the elaborated procedure for the fabrication of coating/steel composite materials used in the construction of interconnects for SOFCs, measurements of their in situ area specific resistance were carried out. The ASR tests of the samples were started after 50 h of pre-oxidation at 1073 K. Fig. 13 shows the dependence of ASR vs. time for the DIN 50049 steel, uncoated and coated with the (La,Sr)CrO_3 during exposure at 1073 K in air and Ar–H_2–H_2O gas mixture. It was found that the electrical resistance of the chromia scale formed on the uncoated steel oxidation in air exceeds the ASR level acceptable for SOFC interconnect material as early as after 160 h, while the same steel oxidized in the Ar–H_2–H_2O gas mixture reaches 0.07 Ω cm^2 after 350 h of continuous monotonic increase. Taking into account the results of the microstructure studies of uncoated DIN 50049 steel presented in the previous subsection, it may be concluded that the existence of cavities in such steel oxidized in air and the formation of a silica phase in a bare substrate during oxidation in the Ar–H_2–H_2O gas mixture reduces the contact surface area between the steel and scale and, in consequence, leads to higher predicted ASR values.

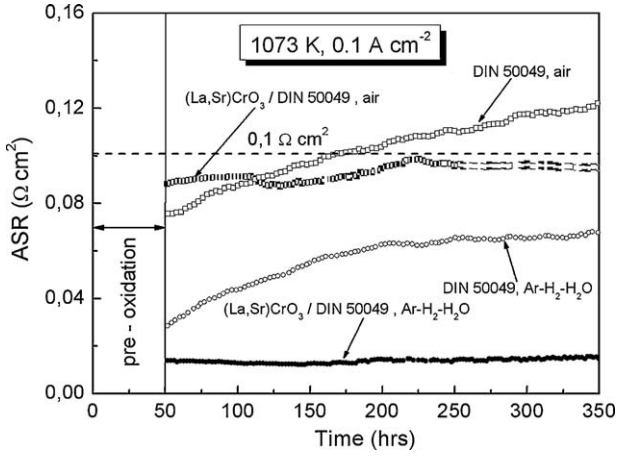

Fig. 13. The time dependence of ASR for uncoated DIN 50049 steel and steel coated with the (La,Sr)CrO_3 thick film during oxidation in air and Ar–H_2–H_2O at 1073 K.

When exposed to air atmosphere at 1073 K, the DIN 50049 steel coated with (La,Sr)CrO_3 exhibits a higher ASR value equal to 0.09 Ω cm^2 after 350 h in comparison with the low electrical resistance of about 0.02 Ω cm^2 measured after the same time in the Ar–H_2–H_2O gas mixture (Fig. 13). The significant difference in ASR values of the studied composite is due to the presence of a thin continuous chromia layer formed at the coating/steel interface during oxidation in air, which simulates SOFC cathode operating conditions. However, unlike the resistance of uncoated steel, which approximately increases according to the parabolic rate law, the resistance of the (La,Sr)CrO_3/DIN 50049 composite reaches a practically constant rate of ca 0.09 Ω cm^2 after around 220 h of oxidation in air. This may most likely be attributed to the precipitation of $SrCrO_4$ during the reaction between the (La,Sr)CrO_3 coating and the Cr_2O_3 layer that forms on the surface of the steel (Table 2). Consequently, the formation of $SrCrO_4$, which has better electrical conductivity than pure Cr_2O_3 [5,49] due to the embedding of strontium ions into the grain boundaries of chromia, significantly improves the electrical properties of the studied composite system, thereby enabling long-term operation of the solid oxide fuel cell. Conversely, the presence of the $SrCrO_4$ phase with a thermal expansion coefficient larger than that of the (La,Sr)CrO_3 coating, as reported in [50], might increase the electrical resistance of the (La,Sr)CrO_3/DIN 50049 composite. However, morphological observations of the studied materials (Figs. 10 and 9(a)) did not show the presence of any voids at the coating/intermediate layer and intermediate layer/steel interfaces. The low and constant resistance of the (La,Sr)CrO_3/DIN 50049 composite during oxidation under low oxygen partial pressure, i.e. in the Ar–H_2–H_2O mixture, is affected by factors such as: the presence of the continuous (Mn,Fe)Cr_2O_4 spinel layer and the $SrCrO_4$ precipitates, the improved adhesion of the reactive layer to the steel core and to the oxide coating, and the modification of transport properties of the intermediate reactive layer. The obtained results indicate that the values of the in situ ASR for the studied coating material exposed to air and the Ar–H_2–H_2O gas mixture at 1073 K are well below the acceptable ASR level for SOFC metallic interconnect materials, which is of the order of 0.1 Ω cm^2.

To evaluate the effectiveness of the applied coatings, Cr-vaporization rate tests of uncoated and coated DIN 50049 ferritic steel were carried out in humid air, under $p_{H_2O} = 9.72 \times 10^{-2}$ atm, at a flow a rate of 2×10^{-6} m^3 s^{-1}, at 1073 K, for 72 h, and under

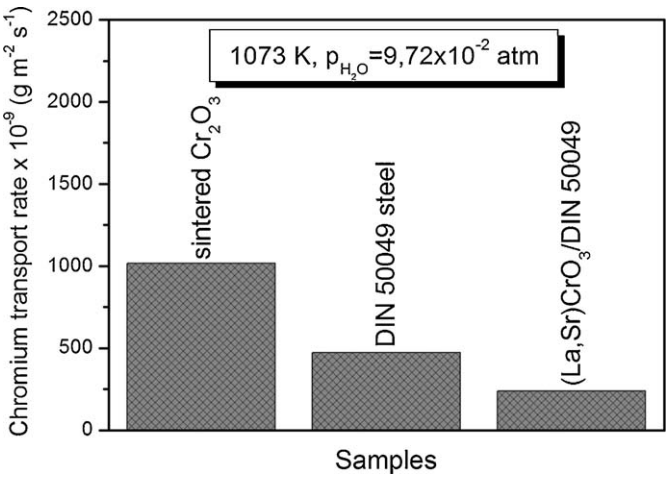

Fig. 14. Chromium transport rate of sintered Cr_2O_3, uncoated DIN 50049 steel and steel coated with the (La,Sr)CrO_3 film at 1073 K in humidified air.

non-equilibrium conditions (unsaturated zone) [15]. Prior to each experiment, all samples were pre-oxidized for 48 h in air at 1073 K. Fig. 14 illustrates the chromium transport rate of the uncoated DIN 50049 steel and the steel coated with the (La,Sr)CrO_3 and the sintered Cr_2O_3 sample as a reference [15]. For the commercial DIN 50049 steel, the loss of mass was over 50% smaller in comparison with the sintered Cr_2O_3 sample. The vaporization rate was considerably reduced by the presence of a thin, continuous $Mn_{1.5}Cr_{1.5}O_4$ spinel layer formed on the outer part of the chromia scale, as indicated by morphological and chemical studies of the oxidized DIN 50049 steel (Fig. 7). Since chromia activity in the $Mn_{1.5}Cr_{1.5}O_4$ spinel decreases to a level below 1, the formation of the spinel on the discussed steel leads to the drop of the rate of mass loss connected with the chromium vaporization effect. The application of the (La,Sr)CrO_3 coatings on the studied DIN 50049 steel decreased the level of vaporization rate of the most abundant chromia species, i.e. $CrO_2(OH)_2$, by ca 50% compared to the oxidized uncoated steel (Fig. 14). These data suggest that the investigated (La,Sr)CrO_3 coating may effectively limit the negative consequences related to the emission of volatile chromium compounds to the cathode site of the SOFC.

While studying the usefulness of the (La,Sr)CrO_3 coating for improving the heat resistance and reducing the electrical resistance of some of the E-brite, Crofer 22APU and AL453 steels, Yang et al. [18] obtained layers with a thickness of around 4 μm using radio frequency magnetron sputtering (RF-MS); despite considerable porosity and numerous microcracks, these layers exhibited low ASR after 250 h of oxidation in air at 1073 K. Among these samples, the (La,Sr)CrO_3/E-brite composite exhibited the best properties. Zhu et al. [26] used the sol-gel method to obtain a (La,Sr)CrO_3 coating on the SAE-AISI 444 ferritic steel. Despite poor compactness, this coating reduces the corrosion rate of the SAE-AISI 444 steel in air at 1073 K in comparison to its uncoated counterpart. In addition, this coating effectively decreased the ASR. Mikkelsen et al. [27], in turn, used PLD laser ablation to deposit a 0.5 μm thick (La,Sr)CrO_3 coating on the surface of the Crofer 22 APU steel; this coating was then oxidized for 500 h in humid air at 1173 K, under isothermal conditions. A significantly lower mass gain was observed for the coated steel compared to the uncoated sample as a result of the slow growth of a chromia-rich multilayer. Gindorf et al. [28] used Vacuum Plasma Spraying and managed to obtain a homogenous and dense (La,Sr)CrO_3 coating on a number of alloys; this coating reduced the negative effects of Cr vaporization by as much as 93%.

The comparison of the results of research by other authors [18,26–28] with our results shows that, despite not preventing the formation of chromia on the surface of the oxidized coating/metal composite, which is inevitable given the ionic conductivity of perovskite compounds based on active elements, using our relatively cost-efficient and simple screen-printing method it is possible to obtain the (La,Sr)CrO_3/DIN 50049 composite material with considerable resistance to oxidation, the desired electrical conductivity, and sufficient ability to absorb gaseous particles of chromium compounds during the oxidation of commercial ferritic steel used as the metallic interconnect in SOFCs. Nonetheless, our research is still in its early stages, and needs to be expanded in order to further decrease the electrical resistance at the ceramics/metal interfaces for longer periods, i.e. thousands of hours. This issue is fundamental for the proper operation of SOFCs.

4. Conclusions

Ultrasonic spray pyrolysis proved to be a useful method for the synthesis of ultra-fine and homogeneous (La,Sr)CrO_3 powders with the desired composition and form of hollow spheres with thin walls to be used in pastes for screen-printing. (La,Sr)CrO_3 perovskite thick films on DIN 50049 steel were fabricated by means of screen-printing with a two-step procedure involving the deposition of paste composed of nanopowder on a metal substrate, followed by annealing in air. The oxidation process of the DIN 50049 steel – uncoated and coated with (La,Sr)CrO_3 – approximately obeys the parabolic rate law at 1073 K in air and the Ar–H_2–H_2O gas mixture. The oxidation rate for the uncoated steel is higher than that for the steel coated with a conducting film, which indicates that the composite material exhibits significant resistance to oxidation in the afore-mentioned thermal conditions. SEM-EDS and TEM-SAD investigations of the ferritic steel coated with the perovskite film after oxidation in different atmospheres revealed the formation of an intermediate, chromia-rich and/or spinel multilayer between the coating and steel. This intermediate layer, which is the result of the structural modification of the coating/steel interface reaction, has been shown to have considerable influence on the area-specific resistance level of the investigated composite materials. The formation of continuous, structurally-modified Cr_2O_3 or (Mn,Fe)Cr_2O_4 spinel layers, both of which include $SrCrO_4$ precipitates, in the (La,Sr)CrO_3/DIN 50049 materials oxidized in air and the Ar–H_2–H_2O gas mixture, respectively, has a beneficial effect on their electrical properties and the chromium-getter barrier. The increase of ASR in the DIN 50049 steel coated with (La,Sr)CrO_3 results from the formation of a thin, continuous Cr_2O_3 layer between the steel and the oxide film in air, while the formation of the continuous (Mn,Fe)Cr_2O_4 spinel layer in the afore-mentioned composite oxidized in the Ar–H_2–H_2O gas mixture has an advantageous effect on its electrical properties. The obtained results prove that the (La,Sr)CrO_3 coatings deposited on the DIN 50049 steel play a protective role as thermal and diffusion barriers against oxidation and chromium vaporization at 1073 K and they are promising candidates for chromia-forming metallic interconnects for planar-type SOFCs.

Acknowledgements

The financial support of the Polish State Committee for Scientific Research (KBN), project no. 4 T08D 014 22, is acknowledged. The authors are grateful to Dr. Ryszard Gajerski and Eng. Jan Oblakowski for their assistance in the preparation of the nanopowders.

References

[1] S.C. Singhal, K. Kendall, High Temperature Solid Oxide Fuel Cells: Fundamentals, Design and Applications, Elsevier, Kidlington, Oxford, 2003.
[2] W.J. Quadakkers, J. Piron-Abellan, V. Shemet, L. Singheiser, Mater. High Temp. 20 (2003) 115.
[3] Z. Yang, K.S. Weil, D.M. Paxton, J.W. Stevenson, J. Electrochem. Soc. 150 (2003) A1188.
[4] J.W. Fergus, Mater. Sci. Eng. A397 (2005) 271;
X. Chen, P.Y. Hou, C.P. Jacobson, S.J. Visco, L.C.D. Jonghe, Solid State Ionics 176 (2005) 425.
[5] T. Brylewski, M. Nanko, T. Maruyama, K. Przybylski, Solid State Ionics 143 (2001) 131.
[6] G. Cabouro, G. Caboche, S. Chevalier, P. Piccardo, J. Power Sources 156 (2006) 39.
[7] N. Shaigan, W. Qu, D.G. Ivey, W. Chen, J. Power Sources 195 (2010) 1529.
[8] T. Kadowaki, T. Shiomitsu, E. Matsuda, H. Nakagawa, H. Tsuneizumi, T. Maruyama, Solid State Ionics 67 (1993) 65.
[9] Z. Yang, G. Xia, S.P. Simner, J.W. Stevenson, J. Electrochem. Soc. 152 (2005) A1896.
[10] X. Montero, N. Jordán, J. Pirón-Abellán, F. Tietz, D. Stöver, M. Cassir, I. Villarreal, J. Electrochem. Soc. 156 (2009) B188.
[11] B. Hua, J. Pu, W. Gong, J. Zhang, F. Lu, L. Jian, J. Power Sources 185 (2008) 419.
[12] K. Hilpert, D. Das, M. Miller, D.H. Peck, R. Weiβ, J. Electrochem. Soc. 143 (1996) 3642.
[13] W.Z. Zhu, S.C. Deevi, Mater. Sci. Eng. A348 (2003) 227.
[14] H. Kurokawa, C.P. Jacobson, L.C. DeJonghe, S. Visco, Solid State Ionics 178 (2007) 287.
[15] T. Brylewski, K. Przybylski, Ann. Chim. Sci. Mat. 33 (2008) 75.
[16] Z. Yang, M.S. Walker, P. Singh, J.W. Stevenson, T. Norby, J. Electrochem. Soc. 151 (2004) 669.
[17] A. Barbucci, P. Piccardo, M.P. Carpanese, M. Viviani, in: Z. Stoynov, D. Vladikova, M. Drinov (Eds.), Portable and Emergency Energy Sources, Prof. Marin Drinov Academic Publishing House, Sofia, 2006, p. 329.
[18] Z.G. Yang, G.G. Xia, G.D. Maupin, J.W. Stevenson:, J. Electrochem. Soc. 153 (2006) A1852.
[19] Y. Larring, T. Norby, J. Electrochem. Soc. 147 (2000) 3251.
[20] Z.G. Yang, G.G. Xia, J.W. Stevenson, Electrochem. Solid State Lett. 8 (2005) A168.
[21] P. Gannon, M. Deibert, P. White, R. Smith, H. Chen, W. Priyantha, J. Lucas, V. Gorokhousky, Int. J. Hydrogen Energy 33 (2008) 3991.
[22] S. Fontana, R. Amendola, S. Chevalier, P. Piccardo, G. Caboche, J. Power Sources 171 (2007) 652.
[23] W. Qu, H. Li, D.G. Ivey, J. Power Sources 138 (2004) 162.
[24] J.W. Fergus, Solid State Ionics 171 (2004) 1.
[25] P. Sujatha Devi, M. Subba Rao, J. Solid State Chem. 98 (1992) 237.
[26] I.H. Zhu, Y. Zhang, A. Basu, Z.G. Lu, M. Paranthaman, D.F. Lee, E.A. Payzant, Surf. Coat. Technol. 177 (2004) 65.
[27] L. Mikkelsen, M. Chen, P.V. Hendriksen, A. Persson, N. Pryds, K. Rodrigo, Surf. Coat. Technol. 202 (2007) 1262.
[28] C. Gindorf, L. Singheiser, K. Hilpert, Steel Res. Int. 72 (2001) 528.
[29] S. Linderoth, Surf. Coat. Technol. 80 (1996) 185.
[30] E.A Lee, S. Lee, H.J. Hwang, J.-W. Moon, J. Power Sources 157 (2006) 709.
[31] A. Kajimura, H. Sasaki, S. Otoshi, M. Suzuki, C. Kurusu, N. Sugiura, M. Ippommatsu, Solid State Ionics 82 (1995) 107.
[32] H.J. Hwang, S. Lee, E.A. Lee, J-W. Moon, Y. Lim, J. Am. Ceram. Soc. 88 (2005) 3275.
[33] K. Przybylski, T. Brylewski, Mater. Trans. 52 (2011) 345.
[34] T. Brylewski, K. Przybylski, J. Morgiel, Mater. Chem. Phys. 81 (2003) 434.
[35] K.T. Wojciechowski, J. Obłąkowski, Solid State Ionics 157 (2003) 341.
[36] K. Przybylski, T. Brylewski, J. Prażuch, Schriften des Forschungszentrums Jülich, vol. 15, Part II, Reihe Energietechnik/Energy Technology, Germany, 2000, p. 741.
[37] S. Chevalier, G. Caboche, K. Przybylski, T. Brylewski, J. Appl. Electrochem. 39 (2009) 529.
[38] P.S. Devi, M.S. Rao, J. Solid State Chem. 98 (1992) 237.
[39] L.V. Azaroff, Elements of X-Ray Crystallography, McGraw-Hill, New York, 1968.
[40] Z. Lu, J. Zhu, Y. Pan, N. Wu, A. Ignatiev, J. Power Sources 178 (2008) 282.
[41] P. Kofstad, High Temperature Corrosion, Elsevier Applied Science Publishers Ltd, London/New York, 1988.
[42] R.A. Rapp, Corrosion 21 (1965) 382.
[43] O. Knacke, O. Kubaschewski, K. Hesselmann (Eds.), Thermochemical Properties of Inorganic Substances, Springer-Verlag, Berlin, 1986.
[44] H. Kurokawa, K. Kawamura, T. Maruyama, Solid State Ionics 168 (2004) 13.
[45] M.G.E. Cox, B. McEnannay, V.D. Scott, Philos. Mag. 26 (1972) 839.
[46] G.J. Yurek, Annual Progress Report, DOE Contract No. DE-AC-02-79ER-10507, Department of Energy, Gaithersburg, MD, 1985, February.
[47] D.H. Peck, M. Miller, K. Hilpert, Solid State Ionics 123 (1999) 59.
[48] S. Miyoshi, S. Onuca, A. Kaimai, H. Matsumoto, K. Yashiro, T. Kawada, J. Mizusaki, H. Yokokawa, J. Solid State Chem. 177 (2004) 4112.
[49] T. Maruyama, T. Inoue, K. Nagata, in: M. Dokiya, O. Yamamoto, H. Tagawa, S.C. Singhal (Eds.), Solid Oxide Fuel Cells (SOFC VI) – Electrochemistry Society Proceedings, vol. 95-1, The Electrochemical Society, Pennington, NJ, 1995, p. 889.
[50] M. Mori, Y. Hiei, N.M. Sammes, Solid State Ionics 135 (2000) 743.